10-1-2018

Brownian Dynamics Of Particles “Dressed” By Chiral Director Configurations In Lyotropic Chromonic Liquid Crystals

A. Martinez

Peter J. Collings
Swarthmore College, pcollin1@swarthmore.edu

A. G. Yodh

Recommended Citation

A. Martinez, Peter J. Collings, and A. G. Yodh. (2018). "Brownian Dynamics Of Particles “Dressed” By Chiral Director Configurations In Lyotropic Chromonic Liquid Crystals". *Physical Review Letters*. Volume 121, Issue 17. DOI: 10.1103/PhysRevLett.121.177801
https://works.swarthmore.edu/fac-physics/366

Brownian Dynamics of Particles "Dressed" by Chiral Director Configurations in Lyotropic Chromonic Liquid Crystals

Angel Martinez,[1] Peter J. Collings,[1,2] and A. G. Yodh[1]
[1]Department of Physics and Astronomy, University of Pennsylvania, Philadelphia, Pennsylvania 19104, USA
[2]Department of Physics and Astronomy, Swarthmore College, Swarthmore, Pennsylvania 19081, USA

(Received 11 August 2018; published 24 October 2018)

We study Brownian dynamics of colloidal spheres, with planar anchoring conditions, suspended in the nematic phase of the lyotropic chromonic liquid crystal disodium chromoglycate (DSCG). Unlike typical liquid crystals, the unusually small twist elastic modulus of DSCG permits two energetically distinct helical distortions (twisted tails) of the nematic director to "dress" the suspended spheres. Video microscopy is used to characterize the helical distortions versus particle size and to measure particle mean-square displacements. Diffusion coefficients parallel and perpendicular to the far-field director, and their anisotropy ratio, are different for the two twisted tail configurations. Moreover, the crossover from subdiffusive to diffusive behavior is anomalously slow for motion perpendicular to the director (>100 s). Simple arguments using Miesowicz viscosities and ideas about twist relaxation are suggested to understand the mean-square displacement observations.

DOI: 10.1103/PhysRevLett.121.177801

The investigation of Brownian dynamics boasts a spectacular history that has produced deep insights about statistical mechanics and about the microscopic environments of diffusing particles [1–4]. Although most of this work concerns the motion of spheres in isotropic media, the effects of anisotropy in Brownian dynamics are proving to be fascinating as well, including the diffusion of anisotropic particles in isotropic fluids [5–10] and particles of all types in anisotropic fluids [11–17].

In this Letter, we explore diffusion of spherical particles in the lyotropic chromonic liquid crystal (LCLC) disodium cromoglycate (DSCG). This background fluid is a nematic liquid crystal (LC) composed of self-assembled achiral rodlike molecular assemblies aligned uniaxially along a director $\mathbf{n}$ [Fig. 1(a)] [18,19]. As in all LC systems, particles in DSCG are expected to exhibit different coefficients for diffusion parallel versus perpendicular to the director field [11,13,14,16,20]. Lyotropic chromonic liquid crystals are different from typical LCs, however, because they easily form twisted or chiral configurations due to their unusually small twist elastic modulus [21–23], an effect also seen in polymer nematic LC systems [24,25]. Thus the local environment for a sphere diffusing in DSCG has a chiral character that depends sensitively on the interplay of bulk elasticity, local geometry, and director boundary conditions. Indeed, it has been shown [26] that spherical colloidal particles with planar anchoring in the nematic phase of DSCG induce localized helical distortions, i.e., "twisted tails" that extend away from the particle parallel to the uniform far-field director $\mathbf{n}_0$ [Figs. 1(b)–1(h)]. The energetics and symmetries of these twisted tail configurations have been studied [26,27], but to our knowledge the effects of chiral distortion of the director on unconstrained particle diffusion have not been considered nor investigated. Moreover, the influence of giant twist elastic anisotropy on relaxation dynamics, broadly defined, has never been explored.

To this end, we employ video and polarized optical microscopy (POM) to investigate diffusion of spheres "dressed" by two classes of chiral director configurations with twisted tails. Diffusion coefficients, parallel and perpendicular to the far-field director, as well as diffusion anisotropy, are revealed to be different for the two classes. In addition, the short-time diffusion dynamics show subdiffusive scaling for motion parallel and perpendicular to the far-field director, and they exhibit anomalously long relaxation times (>100 s) for diffusion perpendicular to $\mathbf{n}_0$. We offer qualitative arguments to understand the measured diffusion coefficient anisotropy based on the Miesowicz viscosities of LCLCs, and we show how giant twist elastic anisotropy can introduce differences in the diffusion behavior of the dressed particles. Our results complement and differ from diffusion measurements, reported in Ref. [16], of heavy silica spheres very close to the substrate without director configuration class identified [see Supplemental Material (SM), Sec. IV [28]]. By positioning particles farther from the substrates, our experiments ameliorate surface drag effects and probe the bulk LC response more effectively. These improvements enable us to uncover substantial variation in subdiffusivity parallel versus perpendicular to $\mathbf{n}_0$, and to distinguish diffusion of particles dressed by different director field configurations. Broadly, the present work elucidates how chiral structures that readily form in LCLCs can affect the dynamics of

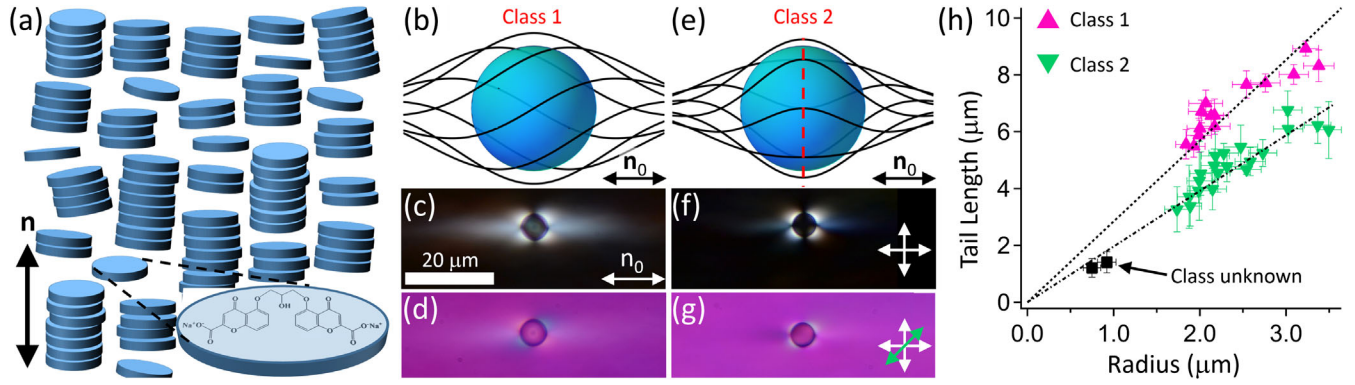

FIG. 1. (a) Illustration of the nematic phase of DSCG. The nematic mesogens are stacks of planklike molecules. (b)–(g) A spherical particle with planar boundary conditions suspended in the uniaxially aligned nematic phase of DSCG induces two distinct twisted tail director configurations: class 1 (b)–(d) and class 2 (e)–(g). Panels (b) and (e) are schematics of twisted director fields (black lines) around the particle. Panels (c) and (f) are crossed-polarized (white arrows) microscopy images. Panels (d) and (g) are crossed-polarized microscopy images with an inserted full wave plate (green arrow). (h) Tail length plotted as a function of particle radius for both symmetry classes. Dotted lines show best proportional fits for each class (see text).

embedded micro- and nanoparticles which, in turn, influences our ability to control particles in LCs for potential device applications [32,33].

Our experiments (see also SM [28]) employ polystyrene divinylbenzene (DVB) spheres in DSCG, with diameters d ranging from 6.5 to 7 μm (unless otherwise specified); typical polydispersity in the source samples is ~2.4%. DSCG molecules are planklike [Fig. 1(a), inset]. The suspensions consist of ~16 wt% DSCG and ~0.015 wt% X100 surfactant in deionized water to prevent the formation of particle clusters. The sample suspensions are loaded into rectangular cells with two rubbed glass substrates, or with one rubbed glass substrate and one rubbed polyimide-coated (SE-7511L, Crystal Diagnostics) substrate. Since the particle density (1.05 g/cm^3) is slightly lower than the density of the DSCG solution (1.0784 ± 0.0032 g/cm^3), the particles are weakly driven toward the upper substrate by gravity. We permit the suspensions to equilibrate for 1.5 days before imaging to ensure that particle proximity to the cell substrate is consistent and does not influence measured diffusion (SM, Sec. IV [28]). The sphere number density is also kept very low to maintain interparticle separations >10 diameters and thereby minimize long-range elastic interactions. Once equilibrated, sample cells are placed within a home-built, temperature-controlled chamber mounted on a microscope stage (SM Fig. 2 [28]). The temperature is held to within 0.1 °C, and 1 h is allowed for temperature equilibration before experiments begin.

Samples are imaged in bright field and POM using a Leica DM IRB inverted microscope with 100x oil objective (N.A. = 1.4). Typically, digital imaging at 60 frames per second over a period of ~15 min is carried out using a CMOS camera (Mikrotron EoSens CL MC1362). Particle tracking uses standard routines written in IDL computer code [34]. The mean-square displacement (MSD) experimental results are typically generated from ~30 video trajectories (~10 trajectories for 3 particles in each class at each temperature). The MSD curves shown represent an average of these trajectories; error bars reported for diffusion coefficients are derived from fits to the average curves.

The resultant particles in the nematic LCLCs are dressed by twisted tails. In contrast to conventional LC systems, wherein spherical particles with planar anchoring generate topological quadrupoles with large splay and bend distortions in the surrounding nematic [15], the splay and bend elastic energies in LCLCs are reduced by twisting the director. As a result, the character of the elastic distortion in the particle vicinity is novel and varied [Figs. 1(b)–1(g)]. One configuration symmetry (class 1), with the director spiraling around the central axis in the same sense on opposite sides of the colloidal particle, is called a chiral dipole and is characterized as an elastic multipole composed of both quadrupole and chiral dipole terms [27,35,36]. The other director configuration (class 2) is globally nonchiral, because the director spirals in an opposite sense on opposite sides of the particle and thereby creates a mirror plane of symmetry [red dashed line in Fig. 1(e)]. Generation of either symmetry class is spontaneous and reversible via melting and requenching of the nematic background phase (SM Fig. 3 [28]). The class 1 configuration is calculated to have the lower energy [26]. In our experiments, we observe both configurations with probabilities ~64% for class 1 and ~36% for class 2 (for more details, see SM, Sec. II [28]), which supports the calculations. We do not observe spontaneous transformation of one class to another without reheating the sample.

Director distortions near the particle are predicted to diminish as the sphere radius is decreased [26]. We measured this effect for the first time and report it in Fig. 1(h) for both classes. An estimate for tail length in each

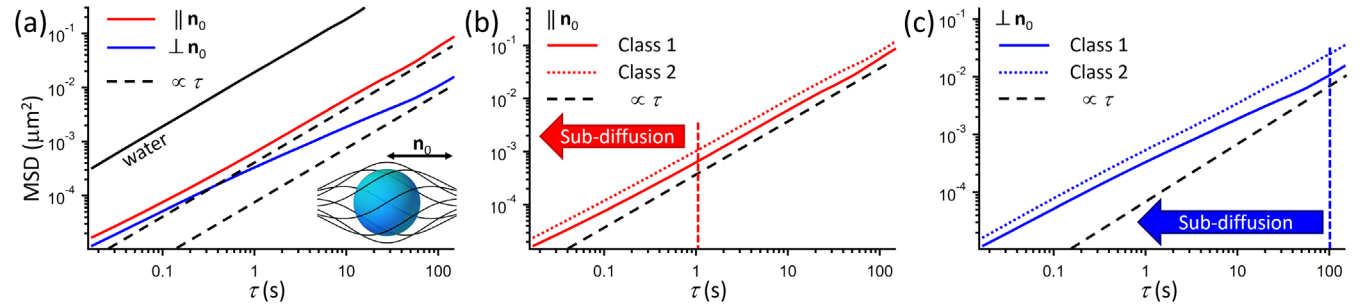

FIG. 2. (a) Mean-squared displacement (MSD) parallel (red) and perpendicular (blue) to $\mathbf{n}_0$ plotted versus lag time for class 1 particles at 23 °C. The black solid line is the MSD for a similar particle in pure water. (b) Comparison of MSD versus lag time for class 1 and 2 particles diffusing parallel to $\mathbf{n}_0$ at 23 °C. (c) Comparison of MSD versus lag time for class 1 and 2 particles diffusing perpendicular to $\mathbf{n}_0$ at 23 °C. Black dashed lines in all plots show normal diffusion (i.e., MSD $\propto \tau$).

class is obtained by fitting the POM image intensity data to a decaying exponential (SM, Sec. III [28]). Even for the smallest particles ($d \approx 1.5$ μm), the distortions never vanish completely. The tail length, defined as the exponential decay length, is ~8 μm (~6 μm) for the class 1 (class 2) particles employed in the diffusion measurements; the tail length is ~2.4 (~1.8) times the particle radius. Thus our data for large diameter particles ($d \gtrsim 4$ μm) are consistent with a theoretical prediction that the director distortion scales with particle radius [26] if the particle is far from the substrate and anchoring at all surfaces is infinitely strong. In short, spherical particles in the LCLC effectively become anisotropic and twisted composite objects when dressed by the surrounding nematic field.

Figure 2 shows our primary MSD versus lag time (τ) results. Figure 2(a) exhibits the salient features of all trajectories. Motion parallel to $\mathbf{n}_0$ is more substantial than perpendicular to $\mathbf{n}_0$, with a comparatively fast crossover from subdiffusive to diffusive behavior. By contrast, this same crossover occurs much more slowly for motion perpendicular to $\mathbf{n}_0$. Figures 2(b) and 2(c) compare the MSD curves parallel and perpendicular to $\mathbf{n}_0$ for class 1 and 2 particles. These data clearly demonstrate that nearly identical colloidal spheres, dressed with the two types of twisted tails, diffuse differently: particles with longer, globally chiral helical tails (class 1) diffuse more slowly than particles with shorter, globally achiral tails (class 2). Long-time diffusion coefficients parallel and perpendicular to $\mathbf{n}_0$ are given in Table I. We also studied the diffusivity temperature dependence and found that (1) diffusivity at long lag times increases with temperature as expected and (2) subdiffusivity persists at all temperatures studied (SM, Sec. V [28]).

The diffusion coefficient anisotropy ratios for the two classes are also shown. Although the dressed spheres do not rotate like ellipsoids, comparison to the diffusion of ellipsoids in isotropic fluids is revealing. Diffusion is slower for motion perpendicular to the ellipsoid long axis, as is the case for the dressed particles. Moreover, the diffusion anisotropy is larger for ellipsoids with larger major/minor axis ratios, just as class 1 particles with larger effective aspect ratios have larger diffusion anisotropies than class 2 particles. However, as expected, the dressed particles are different from ellipsoids. The class 1 and class 2 diffusion anisotropy ratios in Table I, e.g., are significantly larger than for ellipsoids diffusing in 3D, and comparable only to ellipsoids with axis ratios >8 and ~5, respectively, diffusing in quasi-2D [7,37,38]; axis ratios for the dressed spheres based on their measured tail lengths and diameters are ~3.4 and ~2.8, respectively.

Diffusion anisotropy, resulting from the direction-dependent viscous drag, is typical in nematics, but the Stokes drag on a sphere in a nematic LC is very challenging to calculate [15,20,39,40]. It is governed by Ericksen-Leslie equations that connect fluid flow to the director reorientation via elastic and viscous stresses [13,14,41,42]. The coefficients of the viscous stress tensor, the Leslie coefficients, combine to give three Miesowicz viscosities, η_a, η_b, and η_c, for the three shear geometries shown in Fig. 3(a) (a-type geometry), Fig. 3(b) (b-type), and

TABLE I. Diffusion coefficients and diffusion anisotropy ratio for class 1 and 2 particles at 23 °C. These constants are extracted from linear fits to the MSD curves in Figs. 2(b) and 2(c) between lag times of 10 and 150 s for $D_\parallel$ and between 100 and 150 s for $D_\perp$.

	Diameter (μm)	$D_\parallel \times 10^{-16}$ (m^2/s)	$D_\perp \times 10^{-16}$ (m^2/s)	$D_\parallel/D_\perp$
Class 1	6.70 ± 0.16	2.67 ± 0.18	0.515 ± 0.070	5.19
Class 2	6.59 ± 0.14	3.90 ± 0.25	1.12 ± 0.11	3.48

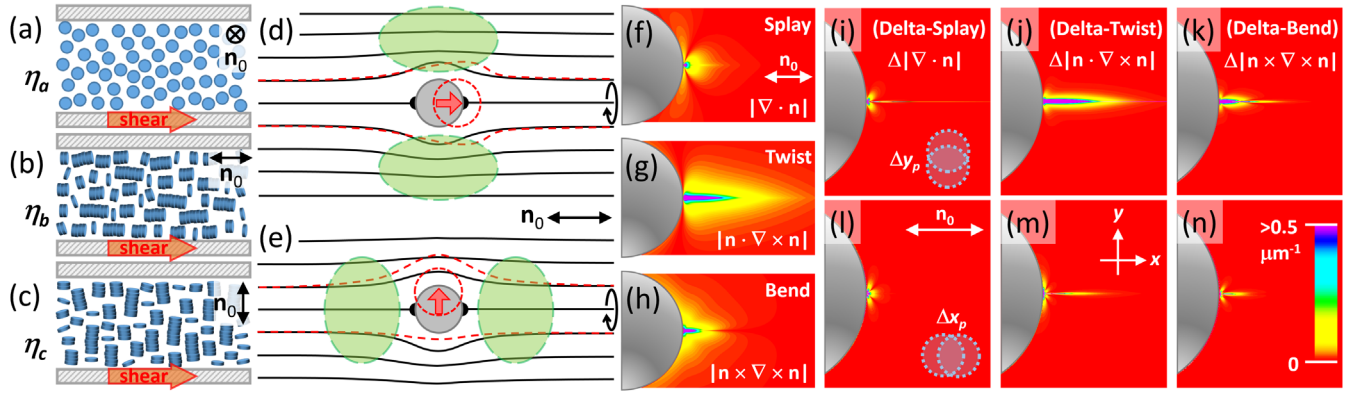

FIG. 3. (a)–(c) Three shear geometries of a nematic LC between parallel plates corresponding to the three Miesowicz viscosities (a) η_a, (b) η_b, and (c) η_c. (d),(e) Cross-sectional schematic of a spherical particle with tangential surface anchoring suspended in a uniaxially aligned nematic. Black lines represent the equilibrium director field for a stationary particle. Red dashed lines represent perturbations in the director field due to colloidal displacements (depicted by red arrows) either (d) parallel or (e) perpendicular to $\mathbf{n}_0$. The green shaded regions are regions of interest when considering the effects of the Miesowicz viscosities (see text and SM [28]). The round arrows to the right indicate that the equilibrium field is axially symmetric. (f)–(h) Calculated (f) splay, (g) twist, and (h) bend distortions as predicted by the theoretical ansatz from Ref. [27]. (i)–(n) Calculated changes in the director fields shown in (f)–(h), due to small particle translations (Δx_p, $\Delta y_p \approx 4.5$ nm) both (i)–(k) perpendicular and (l)–(n) parallel to $\mathbf{n}_0$. The reference frame and color scale insets in (m) and (n), respectively, apply to (f)–(n).

Fig. 3(c) (c-type), respectively. When considering particle diffusion through a uniaxially aligned nematic director configuration, different Miesowicz viscosities make important contributions to the dynamic viscosities, $\eta_{\parallel,\perp}$. For the case of pure (planar) quadrupoles [Figs. 3(d) and 3(e) and SM Figs. 7(a), 8(a), and 8(d) [28]], when the particle moves parallel to $\mathbf{n}_0$, the nematic fluid in the shaded regions of Fig. 3(d) [and SM Fig. 7(a)] experiences mostly b-type shear, since the larger component of the director is parallel to the fluid velocity and perpendicular to the velocity gradient. The smaller director component is perpendicular to the fluid velocity and parallel to the velocity gradient, resulting in a small contribution of c-type shear, so $\eta_\parallel \sim \eta_b + \epsilon\eta_c$ ($\epsilon \ll 1$). When the same particle moves perpendicular to $\mathbf{n}_0$, as in Fig. 3(e) [see also SM Figs. 8(a) and 8(d) [28]], the nematic fluid in the shaded regions experiences mostly c-type shear, since the larger component of the director is perpendicular to the fluid velocity and parallel to the velocity gradient. However, in regions in front of and behind the plane of Fig. 3(e), the larger component of the director is perpendicular to both the fluid velocity and velocity gradient, so a-type shear is also present. The smaller director component is parallel to the fluid velocity and perpendicular to the velocity gradient, so b-type shear gives a small contribution, so $\eta_\perp \sim (\eta_a + \eta_c)/2 + \epsilon\eta_b$.

Typically, for rodlike nematics [14,20,25], $\eta_b < \eta_a < \eta_c$; thus, we expect $D_\parallel > D_\perp$, as observed. These qualitative estimates are useful because they resemble predictions of simple analytical models using the Ericksen-Leslie equations [20]. However, numerical models addressing planar anchoring at the particle surface show that the dynamic viscosities are generally not simple combinations of the Miesowicz viscosities [20]. Furthermore, the relationships between the Miesowicz viscosities and the dynamic viscosities are further complicated by the helicity and large anisotropy of the chiral director distortions (SM Figs. 7 and 8 [28]). Nevertheless, based on the field symmetry and the size of the overall distortions around the spheres, we expect and observe that class 2 particles [SM Figs. 7(a), 7(c), 8(d), and 8(f) [28]] experience an effective viscosity comparatively more similar to that of a pure (planar) quadrupole than the class 1 particles.

Finally, following a phenomenological analysis similar to that in Ref. [16], we consider the origin of the timescales which characterize the crossover from subdiffusive to diffusive behavior. Subdiffusive behavior at short lag times derives from LC-mediated elastic forces due to displacement- and thermally driven fluctuations of the surrounding director field. Director field perturbations due to colloidal displacements cost elastic free energy and generate restoring forces on the particle. Ultimately, they relax back to equilibrium configurations.

The surrounding director perturbations are expected to relax with a characteristic time $t_i \sim l_i^2\eta_i/K_i$, where η_i is a mode viscosity, K_i is an elastic constant, and l_i is a characteristic length scale of the director distortions that must relax back to equilibrium [16,41,42]; the subscript indicates the type of distortion that is relaxing (splay, twist, bend). Strictly speaking, this analysis applies to the relaxation of small periodic fluctuations in the director orientation about the equilibrium field $\mathbf{n}_0$ [21,41,42]. Previously, for diffusing particles, l_i has been assumed to be the particle diameter d [16], but better estimates might consider the regions around the particle wherein distortions change most due to small particle displacements (see below). We posit that crossover from

subdiffusion to normal diffusion will occur on timescales comparable to t_i. To derive these timescales, we use measured estimates for the mode viscosities and elastic constants of DSCG at 23 °C [21], and we choose, for simplicity, $l_i = 2\ \mu$m for all cases. These assumptions provide an estimate t_i for each distortion mode: $(t_{\text{splay}}, t_{\text{twist}}, t_{\text{bend}}) \sim (8, 133, 0.002\ \text{s})$. Note that the twist relaxation time is very long compared to bend and splay as long as the characteristic length scales of the director distortions are comparable; moreover, the timescale of ~100 s for twist relaxation is in rough agreement with the observed crossover time for particle motion perpendicular to $\mathbf{n}_0$.

To understand more deeply how the director field distortions can affect particle diffusion dynamics, we compute the variation of each pure distortion (splay, twist, and bend) due to a small particle displacement (Δx_p, $\Delta y_p \ll d$) either parallel or perpendicular to $\mathbf{n}_0$; here we utilize class 1 spheres because a model describing the distortions is available [27]. The calculated splay, twist, and bend distortions are plotted in Figs. 3(f)–3(h) for a stationary sphere. It is apparent that all modes of distortion are present. In Figs, 3(i)–3(n), we plot the magnitude of the change in these distortions due to small particle displacements (Δx_p, $\Delta y_p \sim 4.5$ nm) perpendicular [Figs. 3(i)–3(k)] and parallel [Figs. 3(l)–3(n)] to $\mathbf{n}_0$. These are the director fluctuations that must relax back to equilibrium after the displacement. Notably, the plots [Figs. 3(i)–3(n)] suggest that the largest changes in $\mathbf{n}$ are associated with twist for particle motion perpendicular to $\mathbf{n}_0$; furthermore, significantly less overall change in $\mathbf{n}$ is observed for motion parallel to $\mathbf{n}_0$. These findings, and the relative timescales for relaxation estimated above, provide strong evidence that long-lived twist distortions play a dominant role in affecting diffusion dynamics in LCLCs.

In summary, the diffusion of spheres in LCLCs is quite different from diffusion in thermotropic LCs. The primary origin of these differences is the unusually small twist elastic constant of LCLCs. Because twist distortions are energetically cheap, the director configuration on each side of the particle is locally chiral, leading to twisted tails that extend much farther away from the particle than the splay and bend distortions of pure quadrupoles. We showed that these differences in twist uniquely affect particle dynamics, both diffusive and subdiffusive motions, as well as the timescales for these processes. Further, differences in diffusion constants and diffusion anisotropy are found for the two chiral director configurations. All of these phenomena are manifestations of the giant twist elastic anisotropy characteristic of LCLCs. Thus, twist effects can be expected to influence our ability to control micro- and nanoparticles in LCs.

This work was supported by National Science Foundation (NSF) under Grant No. DMR16-07378, Materials Research Science and Engineering Center at the University of Pennsylvania (PENN MRSEC) under Grant No. DMR17-20530 including its Optical Microscopy Shared Experimental Facility, and National Aeronautics and Space Administration (NASA) under Grant No. NNX13AL27G. We thank Luana Tortora for supplying the rubbed polyimide-coated glass, and H. Stark, J. Jeong, W-S Wei, A. de la Cotte, X. Ma, T. Turiv, and S. Zumer for useful conversations.

[1] R. Brown, Philos. Mag. **4**, 161 (1828).
[2] A. Einstein, Ann. Phys. (Berlin) **322**, 549 (1905).
[3] J. Perrin, Ann. Chim. Phys. **18**, 5 (1909).
[4] E. Nelson, *Dynamical Theories of Brownian Motion* (Princeton University Press, Princeton, NJ, 1967).
[5] F. Perrin, J. Phys. Radium **7**, 1 (1936).
[6] Y. Han, A. M. Alsayed, M. Nobili, J. Zhang, T. C. Lubensky, and A. G. Yodh, Science **314**, 626 (2006).
[7] Y. Han, A. M. Alsayed, M. Nobili, and A. G. Yodh, Phys. Rev. E **80**, 011403 (2009).
[8] J. Fung and V. N. Manoharan, Phys. Rev. E **88**, 020302 (2013).
[9] M. Molaei, E. Atefi, and J. C. Crocker, Phys. Rev. Lett. **120**, 118002 (2018).
[10] K. Mayoral, T. P. Kennair, X. Zhu, J. Milazzo, K. Ngo, M. M. Fryd, and T. G. Mason, Phys. Rev. E **84**, 051405 (2011).
[11] J.-C. Loudet, P. Hanusse, and P. Poulin, Science **306**, 1525 (2004).
[12] C. D. Muzny and N. A. Clark, Phys. Rev. Lett. **68**, 804 (1992).
[13] R. W. Ruhwandl and E. M. Terentjev, Phys. Rev. E **54**, 5204 (1996).
[14] H. Stark and D. Ventzki, Phys. Rev. E **64**, 031711 (2001).
[15] H. Stark, Phys. Rep. **351**, 387 (2001).
[16] T. Turiv, I. Lazo, A. Brodin, B. I. Lev, V. Reiffenrath, V. G. Nazarenko, and O. D. Lavrentovich, Science **342**, 1351 (2013).
[17] Y. Yuan, A. Martinez, B. Senyuk, M. Tasinkevych, and I. I. Smalyukh, Nat. Mater. **17**, 71 (2018).
[18] P. J. Collings, A. J. Dickinson, and E. C. Smith, Liq. Cryst. **37**, 701 (2010).
[19] D. M. Agra-Kooijman, G. Singh, A. Lorenz, P. J. Collings, Heinz-S. Kitzerow, and S. Kumar, Phys. Rev. E **89**, 062504 (2014).
[20] F. Mondiot, J.-C. Loudet, O. Mondain-Monval, P. Snabre, A. Vilquin, and A. Würger, Phys. Rev. E **86**, 010401(R) (2012).
[21] S. Zhou, K. Neupane, Y. A. Nastishin, A. R. Baldwin, S. V. Shiyanovskii, O. D. Lavrentovich, and S. Sprunt, Soft Matter **10**, 6571 (2014).
[22] J. Jeong, Z. S. Davidson, P. J. Collings, T. C. Lubensky, and A. G. Yodh, Proc. Natl. Acad. Sci. U.S.A. **111**, 1742 (2014).
[23] J. Jeong, L. Kang, Z. S. Davidson, P. J. Collings, T. C. Lubensky, and A. G. Yodh, Proc. Natl. Acad. Sci. U.S.A. **112**, E1837 (2015).
[24] F. Lonberg and R. B. Meyer, Phys. Rev. Lett. **55**, 718 (1985).
[25] S.-D. Lee and R. B. Meyer, Phys. Rev. Lett. **61**, 2217 (1988).

[26] A. Nych, U. Ognysta, I. Muševič, D. Seč, M. Ravnik, and S. Žumer, Phys. Rev. E **89**, 062502 (2014).
[27] V. A. Uzunova and V. M. Pergamenshchik, Phys. Rev. E **84**, 031702 (2011).
[28] See Supplemental Material at http://link.aps.org/supplemental/10.1103/PhysRevLett.121.177801, which includes Refs. [29–31], for further results, experimental details, and theoretical calculations.
[29] P. J. Collings, P. van der Asdonk, A. Martinez, L. Tortora, and P. H. J. Kouwer, Liq. Cryst. **44**, 1165 (2017).
[30] V. M. Pergamenshchik and V. A. Uzunova, Phys. Rev. E **79**, 021704 (2009).
[31] R. Metzler and J. Klafter, Phys. Rep. **339**, 1 (2000).
[32] J. P. F. Lagerwall and G. Scalia, Curr. Appl. Phys. **12**, 1387 (2012).
[33] C. Blanc, D. Coursault, and Emmanuelle Lacaze, Liq. Cryst. Rev. **1**, 83 (2013).
[34] J. C. Crocker and D. G. Grier, J. Colloid Interface Sci. **179**, 298 (1996).
[35] V. M. Pergamenshchik and V. A. Uzunova, Condens. Matter Phys. **13**, 33602 (2010).
[36] V. M. Pergamenshchik and V. A. Uzunova, Phys. Rev. E **83**, 021701 (2011).
[37] J. Happel and H. Brenner, *Low Reynolds Number Hydrodynamics* (Kluwer, Dordrecht, 1991).
[38] S. Bhattacharya, J. Blawzdziewicz, and E. Wajnyrb, J. Fluid Mech. **541**, 263 (2005).
[39] H. Heuer, H. Kneppe, and F. Schneider, Mol. Cryst. Liq. Cryst. **214**, 43 (1992).
[40] A. C. Diogo, Mol. Cryst. Liq. Cryst. **100**, 153 (1983).
[41] P. G. de Gennes and J. Prost, *The Physics of Liquid Crystals*, 2nd ed. (Oxford Science, Oxford, 1993).
[42] S. Chandrasekhar, *Liquid Crystals*, 2nd ed. (Cambridge University Press, Cambridge, Enaland, 1992).